



Snowpack response to directed gas explosions on level ground

Stephan Simioni^{a,*}, Jürg Dual^b, Jürg Schweizer^a

^a WSL Institute for Snow and Avalanche Research SLF, Davos, Switzerland

^b Institute of Mechanical Systems, ETH Zürich, Switzerland



ARTICLE INFO

Keywords:

Avalanche
Avalanche release
Gas exploder
Air pressure
Snowpack accelerations

ABSTRACT

The artificial release of avalanches is an important mitigation measure in avalanche control. The explosion to trigger an avalanche is either produced by igniting solid (or liquid) explosives or a gas mixture. Whereas there have been several studies on the impact of explosives, there is little research on the effect of directed gas explosions on a snowpack. We performed experiments with a prototype gas exploder above snow and measured air pressure at different distances from the point of explosion and accelerations within the snowpack. By measuring along different directions from the point of explosion we assessed the lateral propagation of the pressure wave caused by the directed explosion. Air pressure decreased distinctly with distance from the point of explosion. For example, air pressure was about (6.0 ± 0.2) kPa at 20 m and (0.59 ± 0.02) kPa at 80 m with 1.8 kg of propane-oxygen gas mixture. Within a forward cone of half angle of about 37° , the impact was independent of the direction from the exploder axis. Within the snowpack, accelerations decreased distinctly with depth and distance from the point of explosion as it is observed with explosives. The frequency content of the air pressure signal of the directed gas explosion was similar compared to experimental results previously obtained with solid explosives. We conclude that in the gas exploder axis, the impact of a directed gas explosion is comparable to an explosion with solid explosives with similar energy density. Hence, gas explosions are well suited to artificially trigger snow avalanches. In the future, side-by-side experiments will be needed to further analyze differences and similarities between the effect of gas and solid explosives. Moreover, additional measurements at operational gas exploders will allow further validation of the experimental results.

1. Introduction

The artificial release of avalanches is a key active control measure in avalanche mitigation. It is relatively cheap compared to engineering works such as e.g. constructing a snow shed to protect a road. Moreover, in comparison to snow supporting structures in starting zones the visual impact of remote avalanche control systems is minor. Hundreds of these systems have been installed during the last decade. In principle, they allow avalanche control services to trigger avalanches under any given meteorological conditions and at any time of day. The weather independence is highly relevant as the yield of artificial avalanche release is highest during or directly after a storm (McClung and Schaerer, 2006) and operational constraints often inhibit artificial release during periods of good weather or daylight. However, the point of explosion cannot be adjusted easily for most systems, as the installations are fixed to the ground.

To trigger an avalanche artificially, an explosion is caused by igniting either solid (or liquid) explosives or a gas mixture, either propane-oxygen or hydrogen-oxygen (Berthet-Rambaud, 2009). For

remote avalanche control systems working with gas, the two gases are mixed within a steel pipe that is open on one side and directed with the opening inclined towards the snowpack (Liebermann et al., 2002). The explosion causes a shock and/or subsequently an elastic wave that is propagating outwards from the point of explosion. The air pressure wave is partly transferred to the snowpack depending on snowpack conditions. The mechanical properties and the impedance of snow, the snow-air-interface and the incident angle of the wave influence the part of the wave energy that is transferred to the snowpack (Bouzidi and Schmitt, 2012). The waves generated within the snowpack may then lead to failure and an avalanche might be released.

Since the pioneering works of Mellor (1973) and Gubler (1977), most studies performed on the effects of an explosion on a snowpack in relation to artificial avalanche release focused on near field effects where shock waves are dominant (e.g., Binger et al., 2006; Frigo et al., 2012; Johnson et al., 1994; Johnson et al., 1993). These authors all used solid explosives, investigated shock waves propagating through a snowpack and showed the distinct damping effect of snow.

Recently, Binger and Miller (2016) measured air overpressure above

* Corresponding author.

E-mail address: stephan.simioni@gmail.com (S. Simioni).

a snowpack and snowpack accelerations within a distance of 7 m from the point of explosion, i.e. in the near field. Their study is based on the experiments of Tichota et al. (2010) and Bones et al. (2012). Reported attenuation coefficients of shock and acoustic wave propagation in snow ranged from x^{-1} to $x^{-1.9}$, where x is the distance from the point of explosion. Moreover, Wooldridge et al. (2012) performed stability tests before and after explosions to assess their influence on snowpack stability.

At larger distances from the point of explosion than in the shock range, i.e. larger than about 20 to 30 m, Frigo et al. (2010) performed experiments on a flat study site to assess the effect of an explosion on a snowpack. The most extensive studies in this range were performed by Gubler (1977) and Simioni et al. (2015). The main differences between these studies were that Simioni et al. (2015) measured at different distances simultaneously and performed acceleration measurements at different depths within the snowpack. Hence they could not only describe the decay of the air pressure and snowpack accelerations with distance from the point of explosion, but also the decay with depth within the snowpack. On the other hand, Gubler (1976) provided estimates on the stresses and stability within the snowpack and showed the increased effect by elevating the charge from the snow surface. Cardu et al. (2008) developed a stability criterion for the artificial release of avalanches comprising stress and energy criteria. Simioni et al. (2014) observed weak layer failure during their explosion experiments and reported two different types of failure: one caused by the direct impact of the air pressure wave above the snowpack and one caused by crack propagation initiated closer to the point of explosion.

With regard to ground waves caused by explosions, Ueland (1993) stated that the amplitude of ground vibrations was too low to trigger avalanches at larger distances. Albert and Orcutt (1990) showed that the amplitudes of the acoustic wave transferred to the snowpack were 10 times higher than those of the ground waves transmitted to the snowpack. Suriñach et al. (2011) showed that vibrations caused by the explosion of a gas exploder propagating through the ground may not be sufficient to trigger avalanches at large distances (> 100 m) and that vibrations caused by sound waves propagating through the air and through the snowpack are usually larger than those propagating directly through the ground.

To model the wave propagation in snow Johnson (1982) adapted the model by Biot (1956) to snow and stated the existence of three different wave types. Miller et al. (2011) showed the effect of charge elevation and stress concentrations around a weak layer using a finite element code developed for explosions. Simioni et al. (2014) applied a two-dimensional pseudo-spectral method solving Biot's equations to field experiments using spherical explosives (Sidler, 2015) and showed the propagating wave within the snowpack and failure locations.

In a different context, not related to artificial release, the influence of a snowpack on acoustic wave propagation was investigated. For example, Albert (2001) showed that the acoustic response above a snowpack may vary within a short period of time (hours to days) as snow surface properties change. Albert et al. (2008) reported that acoustic waves above a snowpack were attenuated by as much as – 30 dB within a distance of 100 m.

Whereas many studies on the effect of an explosion on the snowpack were performed using solid explosives as source, no studies exist that systematically investigated the effect of a directed gas explosion on a snowpack. The only studies involving gas exploders were performed by Suriñach et al. (2011) who focused on ground accelerations and Berthet-Rambaud (2009) who developed a test protocol to investigate the effect of gas exploders. Based on near-field pressure measurements, he stated that large differences exist between the shock waves caused by explosions with solids explosives and explosion with various gas mixtures. Gubler et al. (2012) suggested that the impact of a gas explosion is lower than the impact due to the detonation of solid explosives. However, the data provided in the latter two studies are rather sparse. Hence, the detailed effect of gas explosions on a snowpack is

essentially still unknown.

Our aim was to investigate the effect of a directed gas explosion triggered above snow, in particular, in view of the known effect of explosions with solid explosives. Given that operational gas exploders have been successfully applied in avalanche control, we hypothesize that the effect of an explosion of a gas mixture on the snowpack might be similar to the effect of an explosion using solid explosives. We therefore performed measurements following the procedure as previously applied for studying the effect of explosives. We used a mobile experimental gas exploder, a simple steel pipe suspended from a crane on level ground, and measured air pressure above snow and accelerations within the snowpack.

2. Methods

To allow comparison of our measurements with an experimental gas exploder to previous results obtained with solid explosives we essentially followed the same approach as described in Simioni et al. (2015). To assess the propagation characteristics of the air pressure wave and its effect within the snowpack we measured air pressure above snow and accelerations within the snowpack. Measurements were performed along two axes to assess the shape of the impact of a directed gas explosion which is not radially symmetric. In the following we will describe the study site, the experimental setup and data analyses.

2.1. Study site

Experiments were performed near Hinterrhein on a military firing range located at an elevation of 1680 m a.s.l. just north of the Alpine divide in the Eastern Swiss Alps (46.52°N, 9.17°E); it is the same site as was used by Simioni et al. (2015). A flat and level study site was selected to more likely obtain reproducible results. Furthermore, on the level ground, the deployment of the measuring equipment was safe and relatively fast.

2.2. Gas exploder

An experimental gas exploder, manufactured by TAS that produces the Gazex® gas exploder (Liebermann et al., 2002; Stoffel et al., 2015), was used for the experiments. It was suspended from a crane. The gas exploder consisted of a steel pipe that was open at one side (Fig. 1). Its overall length was 2.5 m and its inner diameter 0.8 m. The total volume of the pipe was approx. 1.25 m³. The opening could be closed with a



Fig. 1. View of the gas exploder, suspended from a crane. The pre-tensioned guy wires are connecting the gas exploder to the counterweights. The lower end of the tube is closed by a plastic cover.

Table 1

Summary of all experiments indicating date, test number, mass of the gas mixture, incline of the exploder, angle between the first (gas exploder) and second measurement axis and horizontal distances of the measuring locations from the point of explosion. Gas masses marked with an asterisk (*) are experiments for which no exact mass measurement is available. These masses had to be estimated from the air pressure measurements based on the results of the other experiments. Experiments on 15 June 2016 were performed above bare ground.

Date	Test no.	Exploder elevation	Gas mass	Exploder incline	Angle 2nd axis	Distance (m)					
	(–)	(m)	(kg)	(°)	(°)	X1	X2	X3	Y1	Y2	Y3
10 Mar 2015	1	1.4	0.87*	39	27	17.0	27.1	36.0	16.5	26.4	36.4
10 Mar 2015	2	1.4	0.44*	39	27	17.0	27.1	36.0	16.5	26.4	36.4
10 Mar 2015	3	1.4	0.25*	39	27	17.0	27.1	36.0	16.5	26.4	36.4
10 Mar 2015	4	1.4	0.47*	39	27	17.0	27.1	36.0	16.5	26.4	36.4
10 Mar 2015	10	1.4	0.37*	39	27	17.0	27.1	36.0	16.5	26.4	36.4
10 Mar 2015	11	1.4	0.31*	39	27	17.0	27.1	36.0	16.5	26.4	36.4
10 Mar 2015	12	1.4	0.57*	39	27	17.0	27.1	36.0	16.5	26.4	36.4
11 Mar 2015	1	1.57	0.12*	28	23	12.0	17.2	22.1	11.6	16.3	21.3
11 Mar 2015	2	1.57	0.61*	28	23	12.0	17.2	22.1	11.6	16.3	21.3
11 Mar 2015	3	1.57	0.80*	28	23	12.0	17.2	22.1	11.6	16.3	21.3
11 Mar 2015	4	1.57	0.54*	28	23	12.0	17.2	22.1	11.6	16.3	21.3
11 Mar 2015	13	1.57	1.49*	28	23	12.0	17.2	22.1	11.6	16.3	21.3
16 Feb 2016	1	1.77	0.54	30	37	19.2	34.3	49.2	17.7	32.7	47.6
16 Feb 2016	2	1.77	0.58	30	37	19.2	34.3	49.2	17.7	32.7	47.6
16 Feb 2016	3	1.77	1.09	30	37	19.2	34.3	49.2	17.7	32.7	47.6
16 Feb 2016	4	1.77	1.04	30	37	19.2	34.3	49.2	17.7	32.7	47.6
16 Feb 2016	5	1.77	1.43	30	37	19.2	34.3	49.2	17.7	32.7	47.6
16 Feb 2016	6	1.77	1.41	30	37	19.2	34.3	49.2	17.7	32.7	47.6
16 Feb 2016	7	1.77	1.57	30	37	19.2	34.3	49.2	17.7	32.7	47.6
16 Feb 2016	8	1.77	1.63	30	37	19.2	34.3	49.2	17.7	32.7	47.6
16 Feb 2016	9	1.77	1.82	30	37	19.2	34.3	49.2	17.7	32.7	47.6
17 Feb 2016	1	1.3	1.04	37	29	16.3	25.8	35.1	16.1	26.2	36.1
17 Feb 2016	2	1.8	1.13	36	29	16.3	25.8	35.1	16.1	26.2	36.1
17 Feb 2016	3	1.8	1.30	36	29	16.3	25.8	35.1	16.1	26.2	36.1
17 Feb 2016	4	1.8	1.24	36	29	16.3	25.8	35.1	16.1	26.2	36.1
17 Feb 2016	5	1.8	1.61	36	29	16.3	25.8	35.1	16.1	26.2	36.1
17 Feb 2016	6	1.8	1.61	36	29	16.3	25.8	35.1	16.1	26.2	36.1
17 Feb 2016	7	1.8	1.87	36	29	16.3	25.8	35.1	16.1	26.2	36.1
17 Feb 2016	8	1.8	1.89	36	29	16.3	25.8	35.1	16.1	26.2	36.1
18 Feb 2016	1	1.4	1.36	32	29	16.0	25.6	34.9	15.7	25.9	35.7
18 Feb 2016	2	1.4	1.30	32	29	16.0	25.6	34.9	15.7	25.9	35.7
18 Feb 2016	3	1.4	1.55	32	29	16.0	25.6	34.9	15.7	25.9	35.7
18 Feb 2016	4	1.4	1.50	32	29	16.0	25.6	34.9	15.7	25.9	35.7
18 Feb 2016	5	1.4	1.75	32	29	16.0	25.6	34.9	15.7	25.9	35.7
15 Jun 2016	1	1.4	1.30	34	89	14.1	22.0	28.4	15.3	23.2	30.0
15 Jun 2016	2	1.4	1.27	34	89	14.1	22.0	28.4	15.3	23.2	30.0
15 Jun 2016	3	1.4	1.32	34	89	14.1	22.0	28.4	15.3	23.2	30.0
15 Jun 2016	4	1.4	1.15	34	89	14.1	22.0	28.4	15.3	23.2	30.0
15 Jun 2016	5	1.4	1.12	34	89	14.1	22.0	28.4	15.3	23.2	30.0
15 Jun 2016	6	1.4	1.48	34	89	14.1	22.0	28.4	15.3	23.2	30.0
15 Jun 2016	7	1.4	1.47	34	89	14.1	22.0	28.4	15.3	23.2	30.0
15 Jun 2016	8	1.4	1.49	34	89	14.1	22.0	28.4	15.3	23.2	30.0
15 Jun 2016	9	1.4	1.50	34	89	14.1	22.0	28.4	15.3	23.2	30.0
15 Jun 2016	10	1.4	1.44	34	89	14.1	22.0	28.4	15.3	23.2	30.0
15 Jun 2016	11	1.4	1.48	34	89	14.1	22.0	28.4	15.3	23.2	30.0
15 Jun 2016	12	1.4	1.54	34	89	14.1	22.0	28.4	15.3	23.2	30.0

soft plastic lid using a steel ring and screws to prevent gas heavier than air from flowing out of the tube. The exploder weighed approx. 800 kg. Three suspension points on the exploder were used to hang it up at a certain elevation and incline. The incline was set by adjusting the length of the suspension chains. Two fastening points were installed to guy the exploder to the counter weights which prevented the tube from moving heavily due to the recoil. One or two counter weights, ranging from 1.9 to 2.3 t, were placed laterally (5 to 7 m) and axially (1 to 1.5 m) offset on either side of the exploder. The incline of the pipe was slightly influenced by pulling the gas exploder backwards to reach a certain pretension of the guy wires.

The front bottom of the pipe was elevated between 1.4 and 1.8 m from the snow surface or the bare ground (Table 1). The angle between the inclined exploder and the level snow surface or the ground ranged from 28 to 39° (Table 1). Operational gas exploders are installed with angles of 28 to 48° between the inclined pipe and the snow surface.

Whereas the design of the experimental gas exploder is clearly different from an operational Gazex® gas exploder, it also produces a directed gas explosion using the same gas mixture. We hence consider it

as the best possible setup for a mobile installation.

2.3. Gas

The entire gas installations were provided by the manufacturer of the mobile gas exploder and were the same as used for operational Gazex® gas exploders. However, as the propane-oxygen gas mixture is heavier than air, the opening of the pipe had to be closed as described above. The tube opening was not tightly closed so that the air could flow out while the pipe was filled with gases (Fig. 2). A tight closure would lead to an overpressure in the gas exploder and rupture of the plastic lid and hence total outflow of the mixture before the explosion.

The two different gases were supplied through independent, almost identical setups: The gas flowed from the gas bottle to a larger tank and was set to the required pressure using manual valves and pressure gauges (Fig. 2). After reaching the required tank pressure, the bottle valves were closed to prevent additional gas from flowing into the tank during outflow; this procedure allowed measuring the gas quantity consumed during one experiment. The gas tanks valves were opened



Fig. 2. Pressure reduction tanks for oxygen (blue) and propane (metallic). The gas bottles can be seen in the background. (For interpretation of the references to color in this figure legend, the reader is referred to the web version of this article.)

and gas flowed out for a set period using an electronic trigger. The gas flowed through long pipes to the gas exploder where the two gases were mixed to achieve best explosion efficiency; the mixer was the same as used in operational Gazex® gas exploders. This procedure ensured in combination with check valves at the gas exploder that there was no ignitable mixture in any part of the system except the gas exploder. Immediately after closing the valves the mixture was ignited (see below).

2.4. Gas quantity

A handheld trigger, provided by the manufacturer of the mobile gas exploder, was used to fill the mobile gas exploder and to ignite the mixture with spark plugs that were installed within the pipe. The gas quantity was determined with a time relay to set the opening time of the outflow valves at the gas tanks. With the ignition of the gas mixture, data acquisition was started.

The released gas quantity of either gas was calculated according to the ideal gas law:

$$m_{\text{GAS}} = \frac{\Delta p_{\text{GAS}} V_{\text{tank}}}{R_s T} \quad (\text{kg}) \quad (1)$$

where Δp_{GAS} is the pressure difference (Pa) in the tank before and after releasing the gas, V_{tank} is the volume of the pressure reduction tank (m^3), R_s is the specific gas constant of the respective gas ($\text{J kg}^{-1} \text{K}^{-1}$) and T is the gas temperature (K).

The gas volume at ambient pressure and temperature at the test site was calculated as:

$$V_{\text{GAS}} = \frac{m_{\text{GAS}} R_s T_{\text{atm}}}{p_{\text{atm}}} \quad (\text{m}^3) \quad (2)$$

where p_{atm} and T_{atm} are the atmospheric air pressure (Pa) and the ambient temperature (K) at the test site.

The total gas amount equals the sum of the gas masses or volumes of the two gases oxygen and propane.

On all test days with snow, experiments with different gas volumes were performed. The initial pressure in the tanks was set according to the manufacturer's recommendations. The relative pressure in the oxygen tank was 650 kPa and 140 kPa in the propane tank. The time period (t_0) the gas valves were opened was selected between 0.5 and 3.5 s. Normally, two consecutive tests were performed with the same opening time, i.e. gas volume. While the valves were open the gas pressure in the oxygen tank decreased between 72 and 256 kPa and between 18 and 60 kPa in the propane tank. Outside air temperatures ranged from -3 to -2 °C. The gas temperature in the tanks was

assumed to be equal to the outside air temperature. The oxygen and propane gas masses were determined using the above measurements and the respective gas constants which are $R_{s_{\text{oxygen}}} = 259.8 \text{ J kg}^{-1} \text{ K}^{-1}$ and $R_{s_{\text{propane}}} = 188.5 \text{ J kg}^{-1} \text{ K}^{-1}$ according to Eq. (1). The total gas quantities ranged from 0.12 to 1.8 kg (Table 1); the ratio of the propane to oxygen volumes was approx. 1 to 4. The ambient air pressure p_{atm} , measured several times per day, varied between 829 and 837 hPa. The gas volumes of the two gases in ambient air were calculated using the exact gas measurements and were between 0.43 and 1.51 m^3 ; the maximum gas volumes were hence larger than the exploder volume and our gas masses have to be considered as upper limits. The heat of combustion of propane is 50.3 MJ kg^{-1} . Hence the maximum heat of combustion during the experiments was 23.7 MJ.

For the tests during the winter 2015–2016, exact pressure measurements were available. Since no exact gas measurements were available for the tests during the previous winter, these gas quantities were estimated from the air pressures caused by the explosion measured at various distances above the snowpack and hence back-calculated using the results from the experiments with gas measurements.

On the test day without a snowpack, i.e. over bare ground, the relative pressure was set as in the tests above snow. The time period the valves were opened were 1.5, 2.0 and 2.5 s. These values corresponded to pressure drops in the oxygen tank between 150 and 210 kPa and between 37 and 57 kPa in the propane tank. Using the ideal gas law and ambient pressure and air temperatures, the resulting gas masses ranged from 0.84 to 1.13 kg oxygen and 0.28 to 0.43 kg propane. These gas masses correspond to total gas volumes between 0.67 and 1.26 m^3 .

2.5. Experimental setup

The gas exploder causes a directed explosion (Fig. 3), i.e. it is to be expected that the loading of the snowpack in the axis and in front of the exploder is different than at other angles from this axis. It is therefore not sufficient to perform measurements along the exploder axis only as is usually done when solid explosives with a spherical propagation behavior are tested (e.g. Binger and Miller, 2016). As a consequence, measurements were performed along two axes in a horizontal plane seen from above (Fig. 4). The first axis (X-axis) was in the direction of the pipe; the second axis (Y-axis) was selected such that the snowpack between the two axis was undisturbed and the field of view from the exploder was not obstructed by the counterweights (Fig. 4). For the experiments above snow, the angle between the X-axis (exploder axis) and the Y-axis ranged from 23 to 37° (Table 1) and was limited by the positions of the counterweights. Larger angles would have led to a bias in the measured effect as the counterweights would have reflected the propagating wave partially. For the tests above bare ground, the angle between the two axes was 89° such that the pressure wave from the gas



Fig. 3. View of the gas exploder during an experiment.

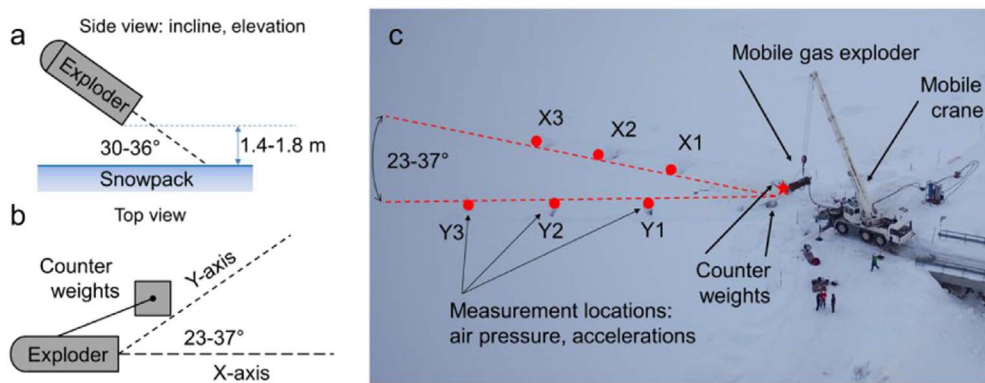


Fig. 4. Experimental set up: (a) Schematic of side view. (b) Schematic of top view. (c) Aerial view of the gas exploder and the crane. The 6 measuring pits are indicated with X1 to Y3.

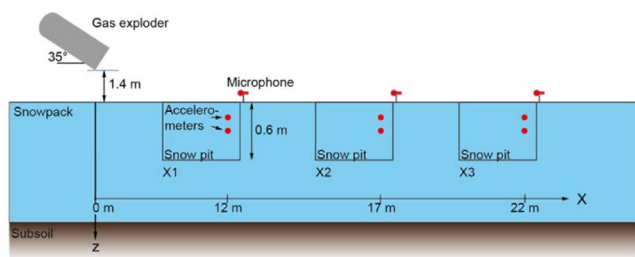


Fig. 5. Longitudinal section of an exemplary measuring layout indicating snow pits X1 to X3 on the X-axis with increasing distance from the point of explosion, gas exploder location, microphones and accelerometers at different distances from the point of explosion and depths z within the snowpack. As an example, the gas exploder was elevated at 1.4 m with an incline of 35°, the horizontal location of the charge is at 0 m, the snow pits X1 to X3 were located at 12, 17 and 22 m horizontal distance from the point of explosion, respectively. The measuring layout was identical on the second axis; figure after Simioni et al. (2015).

explosion could propagate unobstructed behind the counterweights. This was not feasibly above snow.

Three measuring locations were used on each axis at different distances from the point of explosion which was determined as the open tip of the gas exploder (Fig. 5). Differential GPS was used to determine the positions of the gas exploder and the snow pits where the microphones for the air pressure measurement and the accelerometers for snowpack acceleration measurements were installed. The distance of the accelerometers from the microphone and the depth of the sensors within the snowpack were measured manually. The second microphone on the X-axis was installed directly in the axis of the gas exploder. The first and the third microphones were installed slightly offset to obtain an undisturbed snowpack between the gas exploder and the sensors. This offset also resulted in a slight offset of the accelerometers such that there was no disturbed snowpack between the gas exploder and the accelerometers. The accelerometers were installed slightly closer to the point of explosion than the microphones with a few exceptions to prevent any interference of the accelerometer with the post of the microphone. The offset ranged from 5 cm further away from the microphone to 90 cm closer to the point of explosion.

The distances of the microphones from the point of explosion ranged between 11.6 and 49.2 m (Table 1); scaled with the total gas mass the corresponding distances ranged from 9.0 to 90 m kg^{-0.65} (see below for the calculation of the scaling factor).

2.6. Air pressure measurement

Microphones with an upper pressure limit of 34.5 kPa and an upper frequency limit of about 1 kHz (Binger and Miller, 2016; Simioni et al.,

2015) were used to measure near-surface air pressure resulting from the gas explosion at different distances from the point of explosion above the snow surface. Surface air pressure was consistently measured within 3 to 5 cm above the snow surface. Air pressure wave speeds were determined using the arrival times of the air pressure signal at the different microphones. For the experiments above bare ground, the microphones were elevated 30 cm above the ground except for the last four tests when they were mounted 1 m above ground.

2.7. Acceleration measurement

Snowpack accelerations were measured with two-directional accelerometers sealed into foam cylinders to closely match snow density (Table 2) (Simioni et al., 2015). Accelerometers were installed at different depths z within the snowpack and at approximately the same distances from the point of explosion as the air pressure measurements were performed (Fig. 4). Sensors were inserted into the undisturbed snowpack by first cutting out a hole up to one meter back from the snow pit wall.

No acceleration measurements were performed for the experiments above bare ground, as the accelerometers were not suitable for ground acceleration measurement.

2.8. Data acquisition

Data were acquired using the same setup as described in Simioni et al. (2015) with National Instruments cDAQ systems in each snow pit. Data acquisition modules allowed sampling up to 100 kHz per channel simultaneously. Other modules were used to trigger the data acquisition. However, due to the additional axis, six instead of three data acquisition systems were used. Data were transmitted via network cables.

2.9. Data evaluation

2.9.1. Gas mass scaling

With solid explosives, a scaling factor is commonly used to consider different charge masses and their effect on surface air pressure at a certain distance (e.g. Simioni et al., 2015). For a confined gas explosion in a mobile gas exploder, no scaling factor exists. Therefore, a scaling

Table 2
Accelerometer specifications (www.analog.com) (Simioni et al., 2015).

	ADXL203	AD22293	AD22037	ADXL001-70
Range (g)	+/- 1.7	+/- 6	+/- 18	+/- 70
Sensitivity (mV/g)	1000	312	100	24
Resonant frequency (Hz)	5500	5500	5500	> 20,000

factor was calculated for explosions with different gas volumes with the reference gas mass of 1 kg (gas mixture of oxygen and propane, about 3 to 1):

$$x' = x m_G^{-a_G} \quad (\text{m kg}^{-a_G}) \quad (3)$$

The following procedure was used to obtain the best scaling factor: The scaling factor a_G was varied within a certain range. Then, scaled distance x' was calculated for each value of a_G according to Eq. (3). Maximum air pressure values of all experiments along the x-axis were then fitted against these scaled distances x' . The fit with the highest coefficient of determination R^2 determined the best value of a_G , which was subsequently used for gas mass scaling.

The scaling factor was determined using the experiments with precise gas measurements. The factor was then used to estimate the gas masses for the experiments without precise gas measurements based on the maximum air pressure measured at a given distance.

2.9.2. Air pressure decay with distance

The decay of the air pressure with increasing distance was calculated using the measured distances (x) and the maximum air pressure at each location. To include all measurements independent of gas mass, the scaled distances x' were used to fit a power law (Bones et al., 2012; Simioni et al., 2015). All measurements of maximum air pressure with scaled distance from the point of explosion were fitted (separately for the two axes X and Y):

$$p_{\max}^{X,Y} = 10^a x'^{-b} \quad (\text{Pa}) \quad (4)$$

where a and b are the coefficients of the power law and superscripts X or Y refer to the measuring axis and max for the maximum value of the air pressure.

2.9.3. Air pressure increase

In addition to the maximum air pressure, the maximum air pressure derivative $p_{t,\max}$ was calculated, i.e. the largest increase of the air pressure per time that occurs on the first flank of the arriving wave:

$$p_{t,\max} = \left(\frac{dp}{dt} \right)_{\max} \quad (\text{Pa s}^{-1}) \quad (5)$$

where p is the measured air pressure and t is time.

Power laws (with coefficients a_1 , b_1) were also fitted for the decay of the maximum air pressure increase per time $p_{t,\max}$ with scaled distance x' .

2.9.4. Energy equivalent

A simple energy equivalent of the air pressure was used to show the decay of the energy with distance from the point of explosion. This energy equivalent was derived by integrating the squared air pressure:

$$p_{\text{energy}} = \int p^2 dt \quad (\text{Pa}^2 \text{ s}) \quad (6)$$

Power laws (with coefficients a_2 , b_2) were also fitted for the decay of the energy equivalent of the air pressure with scaled distance x' from the point of explosion.

2.9.5. Accelerations and derived parameters within snowpack

Maximum vertical and horizontal accelerations within the snowpack were fitted against the scaled depth z' of the sensors in the snowpack measured from the snow surface in the same way as done with the horizontal distance from the point of explosion. For each distance where accelerations were measured a power law fit for the maximum vertical and horizontal accelerations with scaled depth z' was obtained.

$$a_{s,\max}^{X,Y,\text{pit}} = 10^{a_3} z'^{-b_3} \quad (\text{m s}^{-2}) \quad (7)$$

where a_3 , and b_3 are the coefficients of the power laws.

These relations were then used to fit a power law of the

accelerations with distance from the point of explosion at a certain depth within the snowpack:

$$a_{s,\max}^{X,Y} = 10^{a_4} x'^{-b_4} \quad (\text{m s}^{-2}) \quad (8)$$

where a_4 , and b_4 are the coefficients of the power laws.

Snowpack displacement velocities v and displacements d were determined by integrating the acceleration data once or twice over time, respectively. The maximum values of these quantities were fitted against depth within the snowpack and then against the distance from the point of explosion. The decay exponents of the different quantities were then compared.

The equivalent of the wave energy within the snowpack was calculated by integrating the squared displacement velocity with time:

$$v_{\text{energy}} = \int v^2 dt \quad (\text{m}^2 \text{ s}^{-1}) \quad (9)$$

To compare the decay of the energy with depth within the snowpack to literature values (Capelli et al., 2016), the logarithm of the energy was linearly fitted against the depth. This yielded the following relation between depth and energy:

$$v_{\text{energy}}(z) \sim e^{-b_{\text{en}} z} \quad (10)$$

where b_{en} is the coefficient for the attenuation with depth.

2.9.6. Arrival time and wave speed

The arrival time of the air pressure wave was determined with two algorithms: The STA/LTA method was used, where short and long time averages of the signals are compared and the start is determined as the point where the difference of these averages exceeds a threshold (Withers et al., 1998). In addition, the arrival time was determined by AIC picking (Kurz et al., 2005). With the latter method, the arrival time is determined as the minimum of the AIC function which comprises the logarithm of the variance of the signal starting from the beginning and the end of the signal.

The arrival times at the three measurement locations were used to determine the air pressure wave speeds in the respective distance range. The air pressure wave speed between the gas exploder and the first measurement location was determined using the time when the data acquisition started, which was given by the triggering pulse as zero time. However, we cannot make sure that the zero time coincides with the time of explosion.

3. Experiments and data

During the winter 2014–2015 we performed 13 gas exploder experiments on the test site in Hinterrhein (Table 1). As these were the first experiments with a mobile gas exploder, the experimental setup had not yet been fully developed. Due to the lack of accurate manometers, precise gas volume measurements were not available for these experiments. During the following winter 2015–2016 we performed another 22 gas exploder experiments on three test days at Hinterrhein. In addition, 14 experiments were performed on 15 June 2016 above bare ground. Table 1 compiles the key experimental data, namely date, test number, mass of the gas mixture, incline of the exploder, angle between the first (gas exploder) and second measurement axis and horizontal distances of the measuring locations from the point of explosion.

3.1. Snowpack characteristics

On each of the test days snow stratigraphy and layer properties were recorded by observing a full snow profile (Fierz et al., 2009). In addition, density was determined with either a dielectric probe (Denoth, 1994) or a 100 cm³ density cutter (Proksch et al., 2016).

During the first winter all experiments were performed on 10 and 11 March 2015. Snow depth was approx. 80 cm. The top two centimeters

of the snowpack had previously been moist and hence there was a melt-freeze crust at the surface in the morning on both test days. The snowpack was dry during the first half of the day, but relatively warm with average snow temperatures of approx. $-2\text{ }^{\circ}\text{C}$ on 10 March and $-1\text{ }^{\circ}\text{C}$ on 11 March 2015. During the day the snow temperatures increased and the top 2 cm of the snowpack became slightly moist. This was in particular the case in the second half of the day when most experiments were performed. Average snow density was approx. 335 kg m^{-3} . The snowpack did not include any prominent weak layer.

During winter 2015–2016, we performed all experiments between 16 and 18 February 2016. One manual profile was performed on 16 February 2016; on the two consecutive test days conditions were similar apart from a few centimeters of new snow accumulated on 17 February 2016. Snow depth was about 60 to 70 cm. Average snow density was approx. 285 kg m^{-3} . The snowpack was dry, but warm with an average snow temperature of about $-1\text{ }^{\circ}\text{C}$. As in the previous winter snow stability was rated as ‘good’.

In summary, snowpack characteristics were very similar between our experiments: a rather shallow and warm snowpack with occasionally a slightly moist near-surface layer. Densities were between 200 and 450 kg m^{-3} , slightly increasing or almost constant over depth. In the following, we therefore analyze all measurements jointly since there were now distinct differences in snow conditions.

4. Results

4.1. Gas mass scaling

A single scaling factor was determined for all gas exploder experiments above snow. The best overall scaling factor was $a_G = 0.65$ with $R^2 = 0.997$. This indicates that doubling the gas quantity leads to the same pressure at about 1.5 times the unscaled distance for the gas quantities employed in our experiments.

The overall scaling factor for the experiments above bare ground was lower $a_{G\text{bare}} = 0.4$ with $R^2 = 0.997$. This indicates that a double gas quantity leads to the same pressure at 1.3 times the original distance above bare ground.

4.2. Air pressure above snowpack

A few air pressure measurements were not usable because of microphone malfunction, probably due to loose snow or humidity penetrating the sensor. The air pressure showed a typical sharp increase followed by a steep decrease with a period of negative pressure (or underpressure) (Fig. 6).

The main frequencies of the air pressure signal were in the range of 30 to 40 Hz (Fig. 7a and Fig. 7b). A clear decay of the energy with distance was observed, but the main frequencies did not change. The signals were hardly composed of frequencies above 500 Hz.

Maximum air pressures ranged from 17.5 kPa at a scaled distance of

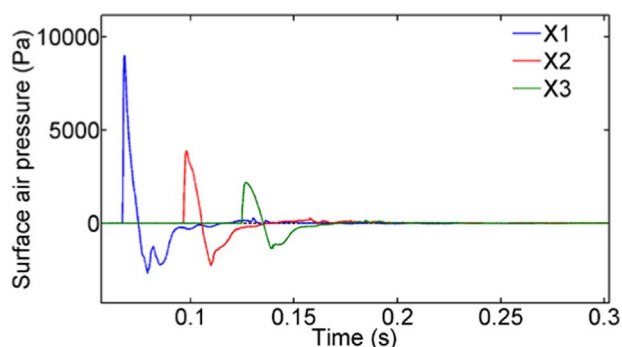


Fig. 6. Example of the air pressure signal at three measuring locations on the X-axis (X1: 16.0 m, X2: 25.6 m, X3: 34.9 m); data from 18 Feb 2016, experiment #5.

approximately $9\text{ m kg}^{-0.65}$ to 0.3 kPa at a scaled distance of approximately $88\text{ m kg}^{-0.65}$. The maximum air pressure for all experiments on all test days with snow decayed distinctly along the X-axis following a power law with an exponent of 1.68 with a standard error (SE) of 0.02 (Fig. 8a and Table 3). Along the Y-axis the maximum air pressure was very similar and also similarly decayed with distance (Fig. 8b and Table 3). As an example, with the largest gas volume used, i.e. 1.8 kg, the maximum air pressure was 6.0 kPa [LCI: 5.8 kPa, UCI: 6.2 kPa] at 20 m and 0.59 kPa [LCI: 0.57 kPa, UPL: 0.61 kPa] at 80 m along the X-axis; the values in brackets indicate the lower (LCI) and upper 95% confidence interval (UCI). On the Y-axis, the maximum pressures at the same distances were 5.5 and 0.56 kPa.

The maximum derivative of the air pressure $p_{,f_{\text{max}}}$ that is reached at the first steep increase of the air pressure ranged from $7.0 \times 10^7\text{ Pa s}^{-1}$ at a scaled distance of $9\text{ m kg}^{-0.65}$ to $5.5 \times 10^5\text{ Pa s}^{-1}$ at a scaled distance of $88\text{ m kg}^{-0.65}$. As the maximum air pressure, the derivative for all test days above snow decayed distinctly with distance from the point of explosion following a power law (Fig. 9a and Table 4).

The equivalent of the air pressure wave energy p_{energy} (cf. Eq. (6)) ranged from $8.45 \times 10^3\text{ Pa}^2\text{ s}$ at a scaled distance of $9\text{ m kg}^{-0.65}$ to $0.59 \times 10^3\text{ Pa}^2\text{ s}$ at a distance of $90\text{ m kg}^{-0.65}$ on the X-axis. The absolute values on the Y-axis were similar. The energy decayed distinctly with distance from the point of explosion, more pronounced than the other air pressure measures, but also following a power law (Fig. 9b and Table 5).

4.3. Accelerations in snowpack

On all test days with snow, snow accelerations were measured at all snow pit locations where also air pressures were measured. In each pit, accelerometers were installed at two different depths below the snow surface. Sensors were buried between 6 and 54 cm below the snow surface. On a given test day, we installed the sensors at approximately the same depths in all snow pits. The sensors were positioned 0.36 to 1.02 m from the snow pit wall into the undisturbed snowpack.

The typical acceleration signals showed a sharp increase at the beginning followed by a sharp decrease and damped oscillation (Fig. 10). At the sensors deeper in the snowpack the accelerations were smaller; the horizontal components were in general smaller than the vertical accelerations. Maximum vertical accelerations within the snowpack on the X-axis ranged from 132 m s^{-2} at $12\text{ m kg}^{-0.65}$ from the point of explosion and approx. 20 cm below the snow surface to 0.8 m s^{-2} at $88\text{ m kg}^{-0.65}$ and approx. 50 cm depth (Fig. 11a). On the Y-axis vertical accelerations reached a maximum of 126 m s^{-2} at $11\text{ m kg}^{-0.65}$ at approx. 20 cm depth and 0.33 m s^{-2} at a distance of $84\text{ m kg}^{-0.65}$ and approx. 50 cm depth (Fig. 12b). Maximum horizontal accelerations ranged from 175 m s^{-2} at a distance of $9.1\text{ m kg}^{-0.65}$ and a depth of approx. 15 cm to 0.2 m s^{-2} at $88\text{ m kg}^{-0.65}$ and a depth of approx. 0.5 m (Fig. 13). On the Y-axis, the maximum accelerations ranged from 95 m s^{-2} at a distance of $11\text{ m kg}^{-0.65}$ and a depth of approx. 15 cm to 0.2 m s^{-2} at a distance of $84\text{ m kg}^{-0.65}$ and a depth of approx. 50 cm. The maximum accelerations decreased distinctly with distance from the point of explosion and depth within the snowpack (Table 6 and Table 7).

The accelerations measured at different depths in each pit decreased rapidly with depth and followed a power law for the vertical and the horizontal component (Table 6). For each axis, the decay with distance from the point of explosion was determined at $0.3\text{ m kg}^{-0.65}$ depth using the power law decay with depth. This depth was chosen as it is a typical fracture depth for artificially triggered avalanches. The accelerations showed a pronounced decay following a power law with distance from the point of explosion at a certain depth within the snowpack for both components and both axes (Table 7).

The main frequencies of the acceleration signal were between 150 and 200 Hz for all depths (Fig. 12). Frequencies above 700 Hz were hardly found in the signal. A clear decay of the energy was observed

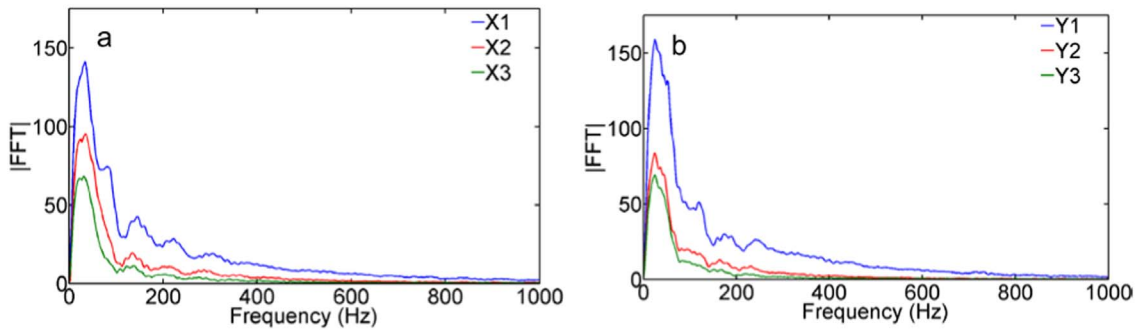


Fig. 7. Example of the air pressure frequency content for the three measuring locations on (a) the X-axis and (b) the Y-axis; data from 18 Feb 2016, experiment #5.

with depth within the snowpack and distance from the point of explosion. The absolute values of the frequency content were lower for the horizontal than for the vertical component.

4.4. Displacement velocities in snowpack

Displacement velocities in the snowpack at the positions of the accelerometers were calculated by integrating the acceleration signal over time. As the integrated noise of the acceleration signal would lead to a non-zero velocity, the start and the end of the signals were manually picked to minimize this effect.

The displacement velocities also showed lower values at larger depths and lower values for the horizontal component (Fig. 14). Maximum vertical displacement velocities ranged from 0.60 m s^{-1} at $9.1 \text{ m kg}^{-0.65}$ distance from the point of explosion and approx. 20 cm depth and $6.5 \times 10^{-4} \text{ m s}^{-1}$ at $88 \text{ m kg}^{-0.65}$ and a depth of approx. 25 cm on the X-axis (Fig. 15). On the Y-axis, the respective values ranged from 0.17 m s^{-1} at $8.3 \text{ m kg}^{-0.65}$ and a depth of approx. 20 cm to $5.7 \times 10^{-4} \text{ m s}^{-1}$ at $84 \text{ m kg}^{-0.65}$ and a depth of approx. 50 cm.

Maximum horizontal velocities ranged from 0.12 m s^{-1} at a distance of $9.1 \text{ m kg}^{-0.65}$ and a depth of approx. 15 cm to $2.4 \times 10^{-4} \text{ m s}^{-1}$ at a distance of $88 \text{ m kg}^{-0.65}$ and a depth of approx. 50 cm below the snow surface on the X-axis. On the Y-axis, the respective values ranged from 0.07 m s^{-1} at $12 \text{ m kg}^{-0.65}$ and a depth of approx. 10 cm to $1.5 \times 10^{-4} \text{ m s}^{-1}$ at $78 \text{ m kg}^{-0.65}$ and a depth of approx. 35 cm.

As for the accelerations, the decay was determined using a power law for each snow pit. The displacement velocities decayed distinctly with depth within the snowpack for all pits for both components and all axes (Table 6). There was a pronounced decay following a power law of the displacement velocities with distance from the point of explosion at the investigated depth of $0.3 \text{ m kg}^{-0.65}$ for both vertical and horizontal components and both axes (Table 7).

Table 3

Power law coefficients for the decay of the maximum air pressures with distance for all experiments above snow and bare ground along the X- and the Y-axis.

	b		a	
	X	Y	X	Y
Snow	1.68	1.65	5.68	5.61
Bare ground	0.99	0.68	5.12	4.51

4.5. Equivalent of wave energy in snowpack

The equivalent of the wave energy in the snowpack, which was calculated from the displacement velocities, increased during passage of the wave to a final value (Fig. 16). The final values at larger depths and for the horizontal component were lower. Fitting the energy equivalent against the depth using power laws showed a pronounced decrease with depth within the snow pits for both components and all axes (Table 6).

Using these power laws to determine the decay with distance from the point of explosion at a certain depth within the snowpack yielded power laws indicating a pronounced decrease from the point of explosion (Table 7).

Using the fitting method by Capelli et al. (2016), the coefficient of the energy decay b_{en} was in the range of 2 to 3.

4.6. Snowpack displacements

Snowpack displacements were calculated by integrating the picked velocity signal over time. Maximum vertical displacements ranged from $3.7 \times 10^{-3} \text{ m}$ at $9.1 \text{ m kg}^{-0.65}$ and at approx. 15 cm below the snow surface to $2.1 \times 10^{-6} \text{ m}$ at a horizontal distance of $88 \text{ m kg}^{-0.65}$ and a depth of approx. 50 cm on the X-axis. On the Y-axis, values ranged from $1.0 \times 10^{-3} \text{ m}$ at $8.3 \text{ m kg}^{-0.65}$ and a depth of approx. 20 cm to $3.6 \times 10^{-6} \text{ m}$ at a distance of $69 \text{ m kg}^{-0.65}$ and a depth of approx. 0.4 m.

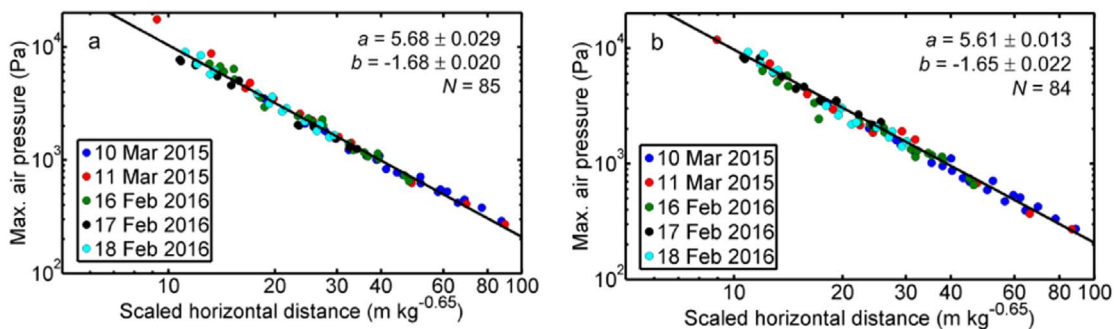


Fig. 8. Maximum air pressure for all test days with scaled distance from the point of explosion on (a) the X-axis and (b) the Y-axis. (For interpretation of the references to color in this figure, the reader is referred to the web version of this article.)

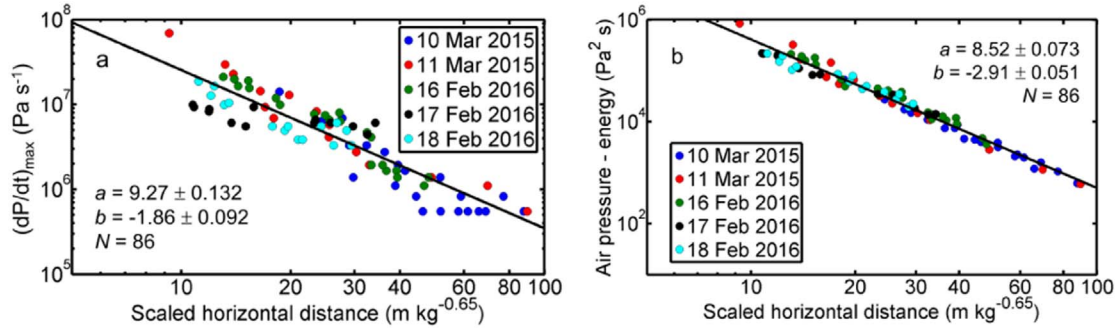


Fig. 9. (a) Maximum air pressure derivatives for all test days with scaled distance from the point of explosion on the X-axis, and (b) energy equivalent of the air pressure for all test days with scaled distance from the point of explosion on the X-axis.

Table 4

Power law coefficients for the decay of the maximum air pressure derivatives with distance for all experiments above snow and bare ground along the X- and the Y-axis.

	b_1		a_1	
	X	Y	X	Y
Snow	1.86	1.50	9.27	8.78
Bare ground		1.18		8.74

Table 5

Power law coefficients for the decay of the equivalent of the air pressure wave energy with distance for all experiments above snow and bare ground along the X- and the Y-axis.

	b_2		a_2	
	X	Y	X	Y
Snow	2.91	2.85	8.52	8.37
Bare ground	1.75	0.87	7.36	5.82

The maximum horizontal displacements ranged from 6.4×10^{-4} m at $9.1 \text{ m kg}^{-0.65}$ and a depth of approx. 15 cm below the snow surface to 4.4×10^{-9} m at a distance of $88 \text{ m kg}^{-0.65}$ and a depth of approx. 50 cm on the X-axis. The range on the Y-axis was from 7.9×10^{-4} m at a distance of $12.6 \text{ m kg}^{-0.65}$ and a depth of approx. 25 cm to 4.3×10^{-9} m at a distance of $88.2 \text{ m kg}^{-0.65}$ and a depth of approx. 0.4 m.

4.7. Air pressure above bare ground

Air pressure was measured at three different distances ranging from 15 to 31 m from the point of explosion and along two axes including an angle of 89° (Table 1). The measurements were not performed at shorter distances because it was expected that the air pressure wave

might interrupt data acquisition as the measuring systems could not be protected in a snow pit.

The maximum air pressure ranged from 13.1 kPa at a distance of $12.7 \text{ m kg}^{-0.4}$ to 4.5 kPa at $17 \text{ m kg}^{-0.4}$ from the point of explosion on the X-axis (Fig. 17a). On the Y-axis (89°), however, the maximum pressure ranged from 6.8 kPa at a distance of $13 \text{ m kg}^{-0.4}$ to 2.6 kPa at $28 \text{ m kg}^{-0.4}$ from the point of explosion (Fig. 17b). The maximum air pressures above bare ground decreased following a power law on both axes (Table 3). As an example, the maximum air pressure using 1.8 kg gas reached 8.4 kPa [LCI: 7.7 kPa, UPI: 9.1 kPa] at 20 m and 2.1 kPa [LCI: 1.6 kPa, UPI: 2.8 kPa] at 80 m from the exploder on the X-axis; on the Y-axis, pressures reached 5.1 kPa [LCI: 4.7 kPa, UPI: 5.4 kPa] and 2.0 kPa [LCI: 1.6 kPa, UPI: 2.5 kPa] at the respective distances.

The maximum of the air pressure derivative was in the range of $2 \times 10^7 \text{ Pa s}^{-1}$ on the X-axis. On the Y-axis, the maximum derivative was $1.9 \times 10^7 \text{ Pa s}^{-1}$ at $20 \text{ m kg}^{-0.4}$ and $8.9 \times 10^6 \text{ Pa s}^{-1}$ at a distance of $28 \text{ m kg}^{-0.4}$. The decay of the air pressure derivative followed a power law on the Y-axis and was similar to the decay of the maximum air pressure (Table 4). On the X-axis, the derivative was only measured correctly at one distance from the explosion and hence no decay could be determined.

The equivalent of the air pressure wave energy p_{energy} ranged from $3.9 \times 10^5 \text{ Pa}^2 \text{s}$ at a scaled distance of $13 \text{ m kg}^{-0.4}$ to $6.4 \times 10^4 \text{ Pa}^2 \text{s}$ at a distance of $27 \text{ m kg}^{-0.4}$ on the X-axis. The absolute values on the Y-axis were $9.1 \times 10^4 \text{ Pa}^2 \text{s}$ at a scaled distance of $13 \text{ m kg}^{-0.4}$ to $2.4 \times 10^4 \text{ Pa}^2 \text{s}$ at a distance of $29 \text{ m kg}^{-0.4}$. The energy equivalent decayed following a power law for both axes showing a pronounced decay (Table 5).

4.8. Influence of exploder incline and elevation

So far we have analyzed all measurements jointly not considering incline and elevation of the exploder with regard to the snow surface.

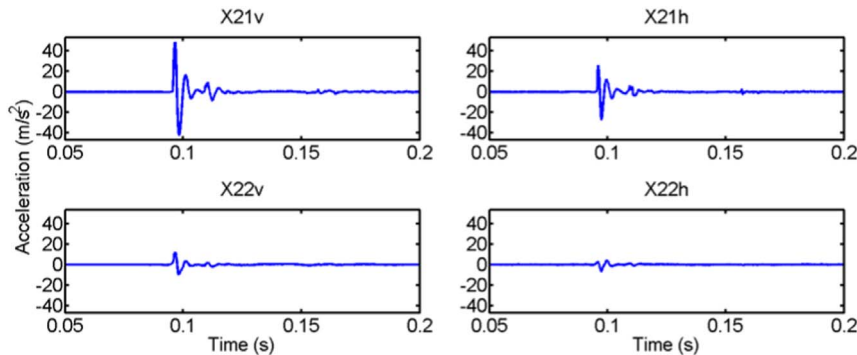


Fig. 10. Accelerations at the system X2 (25.6 m from the point of explosion). The top plots show the top sensors (14 cm below snow surface), the bottom plots the bottom sensor (38 cm below snow surface). Left and right plots show the vertical and the horizontal component, respectively; data from 18 Feb 2016, experiment #5. Positive values indicate accelerations downwards (in z-direction) and away from the point of explosion (in x-direction).

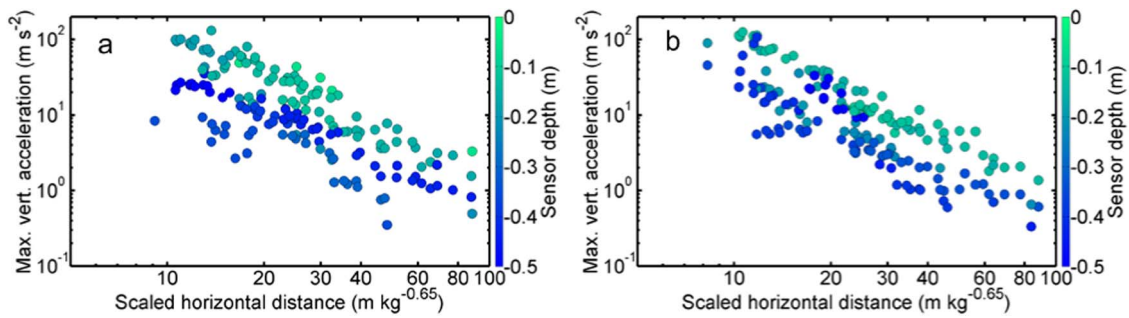


Fig. 11. Maximum vertical accelerations of the snowpack with distance from the point of explosion and depth within the snowpack (color scale) (a) along the X-axis and (b) along the Y-axis. (For interpretation of the references to color in this figure legend, the reader is referred to the web version of this article.)

Comparing all test days with different gas exploder inclines (Table 1), the largest decrease exponents b of the air pressure were observed for the lowest and the largest angle and similar exponents were found for angles between 32 and 37°. However, we only investigated five angles in a relatively narrow range. Moreover, in Fig. 8 the maximum air pressure is plotted with scaled distance; the five test days are shown in different colors. On each of these days, the incline was different. The data scatter around the fit line without showing any trend with regard to the incline.

Similarly, there was neither a consistent nor distinct effect of exploder incline on the decrease of the maximum vertical and horizontal accelerations.

With regard to exploder elevation above the snow surface, the comparison of the maximum air pressure decay exponents for different elevations (Table 1) did not reveal any tendency. Overall, the maximum air pressures for all experiments above snow were similar without apparent trend. Moreover, there was no tendency observable in the maximum vertical and horizontal accelerations for both axes with different gas exploder elevations.

4.9. Effect of snowpack conditions

Snowpack conditions were similar on all test days. The snowpack was well settled, relatively warm, but still dry, except on 10 and 11 March 2015 when the snow surface became slightly moist in the course of the day. However, differences in air pressure and snowpack responses between test days with slightly different snow conditions were minor, showed no tendency and were within the measuring uncertainty.

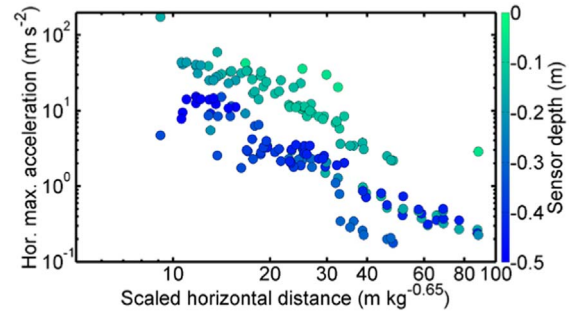


Fig. 13. Maximum horizontal accelerations of the snowpack with distance from the point of explosion and depth within the snowpack (color scale) along the X-axis. (For interpretation of the references to color in this figure legend, the reader is referred to the web version of this article.)

Table 6

Power law coefficients for the accelerations (acc), displacement velocities (vel) and equivalent of the wave energy (energy) with depth within the snowpack for all experiments.

	b_3				a_3			
	X		Y		X		Y	
	vert	hor	vert	hor	vert	hor	vert	hor
acc	1.38	1.34	1.16	0.92	0.13	-0.36	0.19	0.05
vel	1.1	1.1	0.79	0.83	-2.65	-3.3	-2.6	-3.0
energy	1.59	1.14	0.87	0.84	-7.0	-7.4	-6.93	-7.47

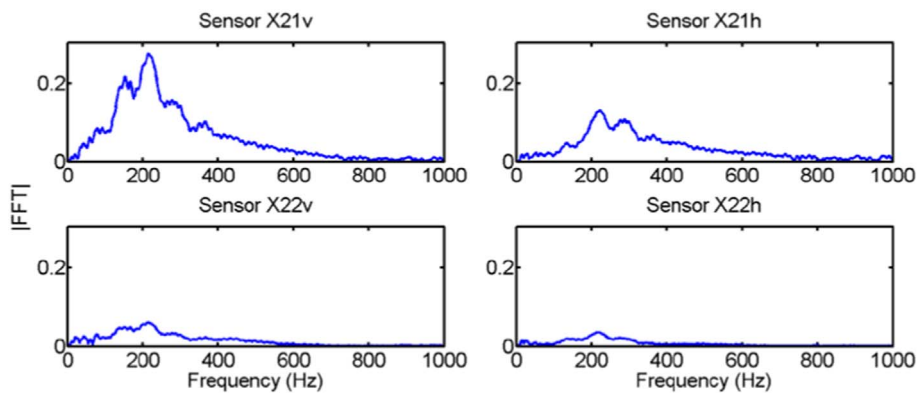


Fig. 12. Frequency content of the accelerations at the system X2 (25.6 m from the point of explosion). The top plots show the top sensors (14 cm below snow surface), the bottom plots the bottom sensor (38 cm below snow surface). Left and right plots show the vertical and the horizontal component, respectively; data from 18 Feb 2016, experiment #5.

Table 7

Power law coefficients for the accelerations (acc), displacement velocities (vel) and equivalent of the wave energy (energy) with distance from the point of explosion for a certain depth within the snowpack for all experiments (mean).

	b ₄				a ₄			
	X		Y		X		Y	
	vert	hor	vert	hor	vert	hor	vert	hor
acc	1.96	2.68	2.19	2.82	3.7	4.15	3.84	4.44
vel	2.19	2.96	1.73	1.77	1.07	1.59	0.19	0.01
energy	3.75	4.68	2.81	2.27	-0.94	-0.11	-2.59	-3.79

4.10. Air pressure wave speeds

Air pressure wave speeds were calculated from the arrival times and the distances between the microphones. The mean air wave speeds measured for each test day were between 322 and 333 m s⁻¹. Air pressures between the spark plugs in the gas exploder and the first sensor location on each axis were lower – indicating a measurement problem (see below). There were no speeds above the speed of sound observed within the range of reliable measurements.

5. Discussion

5.1. Gas quantities and gas scaling

The gas quantities we calculated using the ideal gas law ranged from 0.43 to 1.51 m³. However, the volume of the gas exploder was approx. 1.25 m³. This means at least for the larger gas volumes, that the gas mixture had partly flown out of the gas exploder. This is possible because the pipe was not tight at the front. If the pipe had been closed tightly, an overpressure in the pipe would have resulted possibly causing the pre-blast failure of the plastic cover. Furthermore, this overpressure would not have been representative for the conditions found with operational gas exploders.

The gases flowed very rapidly into the gas exploder with a maximum speed of approx. 0.55 m³ s⁻¹. This probably led to turbulent flow behavior in the gas exploder. It is hence not clear and not measurable how the gases mix and flow within the exploder. As the gases enter in the back half of the pipe, one may assume that mainly atmospheric air will be pushed out of the pipe. We suspect that always the same proportion of the gas flowed out of the pipe as the gas mixture is heavier than atmospheric air. However, for several reasons it was not possible to check the composition of the gas mixture within the gas exploder. Besides the issue of measuring a gas mixture that is highly explosive, the gas mixture will flow rapidly within the gas exploder making it

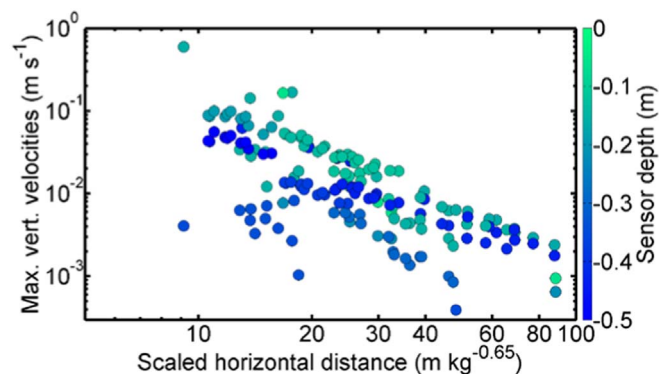


Fig. 15. Maximum vertical velocities of the snowpack with distance from the point of explosion and depth within the snowpack (color scale) along the X-axis. (For interpretation of the references to color in this figure legend, the reader is referred to the web version of this article.)

almost impossible to interpret the information about the gas mixture that is changing with time.

While determining the gas scaling factor we did not consider that obviously part of the gas mixture was flowing out of the pipe. However, as the fit between gas masses and maximum air pressure was good, the effect of the outflowing gas seems to be of little importance. If the loss of gas had been more prominent for volumes larger than 1.25 m³, the volume of the gas exploder, the deviation from the fit would have increased for the larger volumes, which was not the case. Therefore, we assume that always the same proportion of gas flowed out of the pipe, hence the gas masses we calculated might systematically be too large. This means that the pressure values represent upper limits and rather belong to lower gas masses – still, the gas leak does not affect our principal findings of the effect of a directed gas explosion on the snowpack. In any case, it is not fully clear how the gas masses used with our prototype exploder compare to those used in operational exploders.

The gas scaling factor was determined using the maximum air pressures and gas masses for those experiments, where exact gas measurements were available. The best-fit scaling factor above snow was 0.65. This value is almost twice as large as the scaling factor used for solid explosive with a spherical expansion which is commonly assumed to be 1/3 (Cooper, 1996). A factor of 1/3 was used in previous studies (Binger and Miller, 2016; Bones et al., 2012) and Simioni et al. (2015) showed that this assumption is valid for experiments with solid explosives above snow. The difference between the scaling factors may be due to geometrical effects: The gas exploder creates a directed explosion which is clearly different from a spherical expansion, but rather a mixture between plane and spherical expansion. Therefore, it is plausible that the scaling factor for a directed gas explosion is larger than for

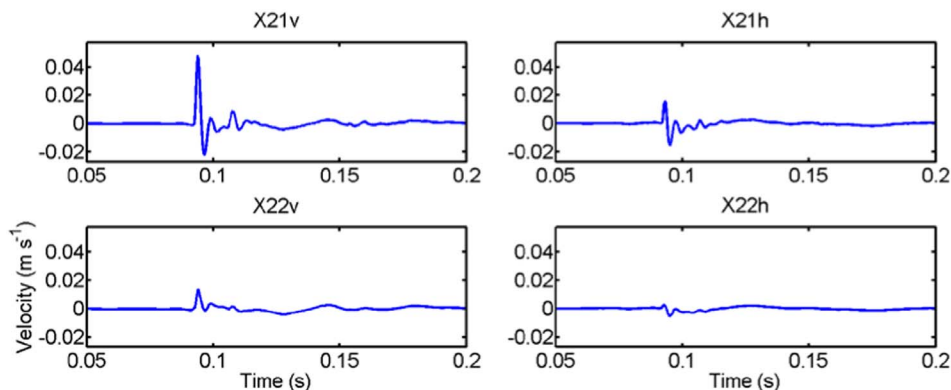


Fig. 14. Velocities at the system X2 (25.6 m). The top plots show the top sensors (14 cm below snow surface), the bottom plots the bottom sensor (38 cm below snow surface). Left and right plots show the vertical and the horizontal component, respectively; data from 18 Feb 2016, experiment #5. Positive values indicate velocities downwards (in z-direction) and away from the point of explosion (in x-direction).

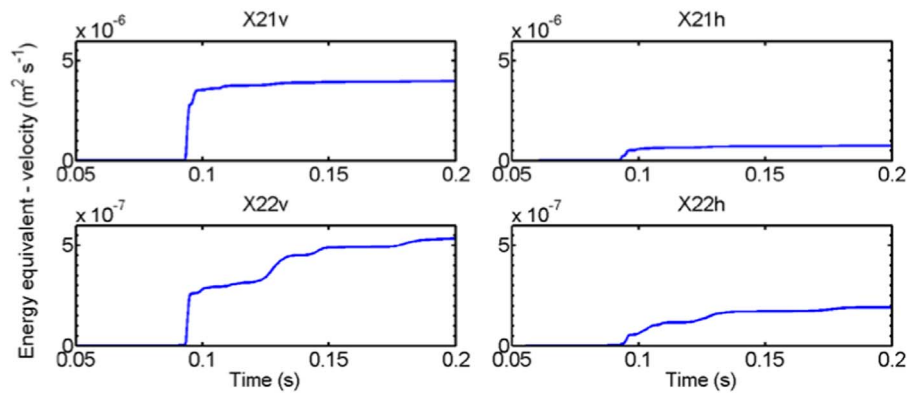


Fig. 16. Energy equivalent derived from the velocities at the system X2 (25.6 m). The top plots show the top sensors (14 cm below snow surface), the bottom plots the bottom sensor (38 cm below snow surface). Left and right plots show the vertical and the horizontal component respectively. Note the different scales on the ordinates; data from 18 Feb 2016, experiment #5.

a spherical explosion as found with solid explosives.

We did not consider that snowpack conditions slightly varied during our experiments while determining the scaling factor, since Simioni et al. (2015) did not find a relevant difference for the air pressure propagation for the limited range of snow conditions they encountered.

The best scaling factor for the experiments above bare ground was 0.4. The difference to the scaling factor above snow is related to the different properties of the underlying material. The other setup parameters (elevation, incline, gas mixture) were in the same range as for the experiments above snow.

5.2. Air pressure

We measured a decay of the air pressure proportional to $x^{-1.68}$ in the exploder axis (Table 3). This is within the range of values reported by Simioni et al. (2015) for solid explosives ($x^{-1.1}$ to $x^{-2.1}$). The values were higher than what Gubler (1976) reported, slightly higher than what Ingram (1962) and Mellor (1973) observed, but in excellent agreement with the results from Albert and Hole (2001). The values between $b_{\text{airp}}^X = 1$ and $b_{\text{airp}}^X = 2$ show that the decay is more distinct than for a spherical expansion ($b = 1$). As the decay of the air pressure is similar up to the investigated angle of approx. 37° from the exploder axis to the side, we conclude that the air pressure and its decay is similar to that of an explosion caused by a solid explosive, at least within an aperture angle of about 74° . The air pressure derivative decayed similarly with distance from the point of explosion as the maximum air pressure itself (Table 4).

There was considerable scatter in the air pressure measurements; the standard error of the exponent was 0.02 with lower and upper 95% confidence interval of -1.71 and -1.64 , respectively. Many sources of error may contribute to the scatter: variations in meteorological conditions, sensor location (distance), gas mass determination, snow conditions, gas mixture and ignition, and mounting (stiffness of system) and position of exploder.

The calculated equivalent of the air pressure wave energy as well decreased distinctly with distance from the point of explosion with a power law exponent of about 2.9 ($x^{-2.9}$) (Table 5). As the energy is proportional to the pressure amplitude squared, this decrease with distance is plausible. We are not aware of any previous studies our results on the energy equivalent could be compared to.

The air pressure above bare ground decreased less distinctly ($b_{\text{airp}}^{X,\text{bare}} = 0.99$) with distance from the point of explosion than above snow ($b_{\text{airp}}^X = 1.68$) (Table 3). The decay above bare ground was close to the decrease of a spherical wave although the directed explosion is not causing a spherical expansion. The lower exponent above bare ground is rather related to the effect of the different surface properties of snow vs. bare ground. The snowpack absorbs part of the air pressure wave because its impedance – would it be a continuum – is closer to that of air than the impedance of soil. In addition, the open pores of a snowpack further decrease the reflectivity of the incoming wave.

The maximum air pressures above bare ground at 89° from the exploder axis were smaller than in the exploder axis. For example, at $13 \text{ m kg}^{-0.4}$, the maximum air pressure was 13.1 kPa on the X-axis and 6.8 kPa on the Y-axis. However, the decrease along the Y-axis was much less pronounced with $b_{\text{airp}}^{Y,\text{bare}} = 0.68$ compared to the decrease on the X-axis with $b_{\text{airp}}^{X,\text{bare}} = 0.99$. This means that at a distance of $93 \text{ m kg}^{-0.4}$, the air pressure on the Y-axis was as large as on the X-axis. Due to the inclined tube the amplitude decay perpendicular to the pipe axis is closer to the decay of a cylindrical wave, whereas the decay along the pipe axis seems to reflect more spherical wave expansion. Whereas the absolute values close to the point of explosion are significantly higher on the X-axis, the values are equal at large distances. Isolines indicating the same pressure will be bulb-shaped close to the explosion but change to a circle at large distance.

The counterweights inhibited experiments at other angles than up to 37° from the exploder axis and below approx. 85° from the axis. It would have been a possibility to build a fixed foundation in the soil. This would, however, have prevented experiments at different

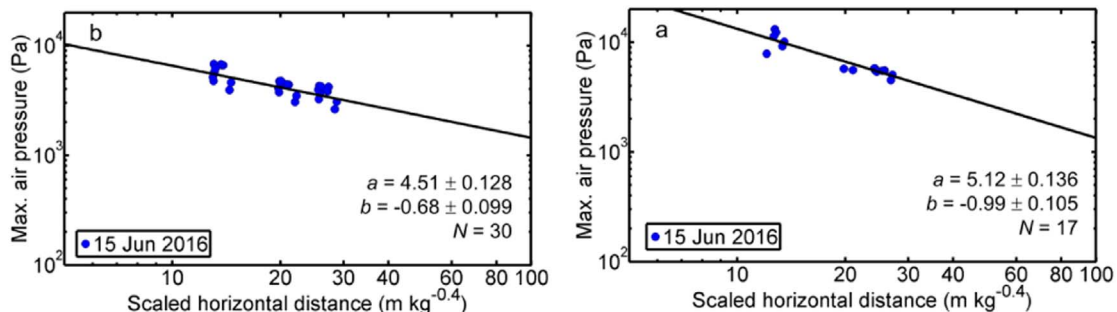


Fig. 17. Maximum air pressures above bare ground with distance from the point of explosion (a) along the X-axis, and (b) along the Y-axis (at 89° from X-axis).

locations. Instrumenting the experiments to the back (180° from the gas exploder axis to the front) was not feasible due to the embankment of the road.

5.3. Accelerations

On average, the decay with depth within the snowpack at all three distances from the point of explosion was proportional to $x^{-1.38}$ (Table 6). Our results are in good agreement with the results of Binger and Miller (2016) who measured at much closer distances and under conditions they called ‘hard slab snow’. However, scatter in our results was large and caused by the complexity to accurately position the sensors relatively to each other, by the difference between sensor and snow density which existed for layers that did not match the average sensor density of 200 kg m^{-3} , and the correct coupling of the sensor within the hole.

The maximum vertical accelerations behaved similarly with distance from the point of explosion within the aperture of up to 37° from the exploder axis, with $b_{\text{acc}} = 1.96$ in the gas exploder axis and $b_{\text{acc}} = 2.19$ on the Y-axis (Table 7). The maximum horizontal accelerations decreased more distinct with distance than the vertical component ($b_{\text{acc}} = 2.68$ and $b_{\text{acc}} = 2.82$ for the X- and Y-axis, respectively). These values are in good agreement with the results for hard slab snow reported in Binger and Miller (2016). The average decrease was more pronounced than reported in Simioni et al. (2015), but scatter was equally large. The maximum horizontal accelerations were smaller. The observed decay is in good agreement with the observations by Bones et al. (2012). Suriñach et al. (2011) did not provide a relation for the decay with distance but reported a decreasing tendency with distance from the point of explosion. They measured at distances larger than 130 m and observed ground accelerations that were in the range of 0.01 to $1 \times 10^{-5} \text{ m s}^{-2}$ which seem plausible compared to our observations.

5.4. Displacement velocities

Velocities within the snowpack showed a pronounced decay with depth for all pits, more distinct for the vertical than for the horizontal component (Table 6). However, scatter was large due to the same reasons as described above for the accelerations.

Velocities within the snowpack decayed more pronounced with distance from the point of explosion at a certain depth than reported by Simioni et al. (2015) (Table 7). Vertical velocities decayed less distinctly than horizontal velocities but the decay or their values were similar. Velocities on the Y-axis, out to 37° from the X-axis, decayed less distinctly than velocities on the exploder axis. The decay was more pronounced than reported by Gubler (1976).

5.5. Equivalent of the wave energy in the snowpack

The energy equivalent, calculated from the snowpack velocities, decreased more pronounced on the X-axis than on the Y-axis for each pit with increasing depth from the snow surface (Table 6). The vertical component decreased slightly more distinct than the horizontal component.

The energy equivalent decreased distinctly with distance from the point of explosion at a given depth (Table 7). We are not aware of any previous results to compare our results of energy equivalent to.

The values of the power law exponent obtained with the method using the fitting to the semi-log-plot ($b_{\text{en}} \approx 2$ to 3) were higher than those reported in Capelli et al. (2016) ($b_{\text{en}} \approx 0.35$ to 1.2). The reason is that Capelli et al. (2016) performed their experiments under lab-conditions with a single grain type, a well-known geometry and plane waves. In addition, our results comprise the effects of an inhomogeneous multi-layered snowpack causing reflections and non-planar propagation. Furthermore, the wave does not hit the sensors

perpendicular to the snow surface and hence a wave arriving at a sensor will not be the same wave that arrives at a lower sensor. The wave arriving at the lower sensor will be transmitted from the air to the snowpack at a shorter distance from the point of explosion. Attenuation measurements in snow seem to be extremely delicate to perform and hence previously reported values vary significantly, in the range of 0.05 to 3.5 dB cm^{-1} (Capelli et al., 2016).

5.6. Displacements

Maximum displacement ranged between 10^{-3} m for measurements close to the surface and close to the point of explosion to 10^{-6} m for larger distances and depths within the snowpack. This is in good agreement with the results of Gubler (1976) and Simioni et al. (2015). No fit parameters for the power law are given for the gas exploder experiments, since the absolute displacement values were too small to allow any conclusions based on a power law fit.

5.7. Frequency content

The main frequencies of the air pressure signals of the gas exploder experiments (30 to 40 Hz) are in good agreement with the solid explosive experiments (~40 Hz) performed by Simioni et al. (2015). However, the main frequencies of the accelerations within the snowpack were much higher for the gas exploder experiments (~200 Hz) than for the solid explosive experiments (~40 Hz). As the air pressure frequencies for both types of experiments were similar, it is expected that under given snowpack conditions, the frequency content within the snowpack should be similar, too. The observed difference may be related to snow depth. The snow depth reported in Simioni et al. (2015) was more than double of the depth observed during our experiments. It seems that the frequency content reflects the vibration behavior of the entire snowpack. Low frequencies and long wave lengths combined with shallow snow depth would support this assumption. The decay of both the air pressure and the acceleration signals was frequency-dependent. The lower frequencies decayed less distinctly with distance than the higher frequencies. In snow, this was expected due to non-elastic effects.

5.8. Influence of gas exploder incline and elevation

Gas exploder incline was measured for the setup before an explosion. Due to the recoil and variable tension of the guy wires between test days, the effective angle at the time of impact may have slightly varied from the initial measurements. The greatest decrease of the air pressure with distance from the point of explosion was obtained with the lowest gas exploder incline (28°). This is counter-intuitive as one would expect that with a large incline and a directed explosion, pressures would be high close to the surface and decrease rapidly with distance. However, when looking at the absolute air pressure values with distance, the differences were small. Furthermore, as pointed out above, there is some uncertainty with regard to the incline itself. We conclude the effect of the exploder incline – at least in the relatively narrow range of angles we investigated – to be of minor importance for maximum air pressure and its decay with distance from the point of explosion.

There was no influence of the gas exploder elevation observed. Compared to the size of the gas exploder and the distances where we performed measurements, an increase in elevation of approx. 50 cm does obviously not result in significant differences in air pressure.

5.9. Snow conditions

The snowpack during the two experimental periods was rather shallow with snow depths between 60 and 80 cm. Densities were rather high compared to snowpacks usually found when avalanches are

triggered artificially and near surface layers often consist of new snow. Furthermore, all experiments were performed under dry, warm snow conditions with only occasionally a slightly moist snow surface (in March 2015). Hence, in our limited data series we did not have significantly varying snow conditions between or during test days.

We did not observe significant differences in the decrease of the air pressure with distance from the point of explosion due to the snow conditions we encountered. In general, one would expect that snow conditions play an important role, in particular when comparing a dry to a wet snowpack. It is known that the effect of solid explosives in wet snow with regard to artificial triggering is much smaller than in dry snow due to higher attenuation in wet snow (e.g., Albert, 1983). However, we only had relatively small differences in snow conditions during and between our test days. Their effect might be hidden in the overall measurement errors. The main difference in snow conditions we encountered was the volumetric liquid water content of the surface layer, which was low (i.e. in the range of 0 to 3%). In March 2015 a melt-freeze crust became slightly moist in the course of the day. However, the liquid water content was low so that the hardness of the crust did hardly change. Still, one would expect some effect due to changes in the topmost layer. Indeed Albert and Hole (2001) stated that changes in snowpack conditions considerably influence wave propagation above snow, i.e. that also the transmission of the air pressure wave into the snowpack will vary with differences in snowpack conditions. These changes can happen within the course of a day, as described above, and may in fact explain some of the scatter observed for the air pressure and the derived parameters with distance from the point of explosion.

As for the air pressure, no large differences were observed for the quantities measured within the snowpack with different snowpack conditions. The observed differences did not show any clear tendency. Hence, the layering and other properties of the snowpack may have had as much an influence as slight changes at the snow surface. Many different layers will cause stronger reflections and hence more pronounced attenuation measured between two sensors than a snowpack with fewer similar layers due to impedance differences caused by the first. Ice lenses and crusts in combination with other, less dense snow layers will reflect a large part of the energy due to large impedance differences.

An alternative explanation for the low effect of snow properties observed in our limited dataset on air pressure attenuation and related quantities is that the previously reported low impact under wet-snow conditions may be due to the fact that explosions were triggered within wet snow (e.g., Gubler, 1977; Johnson et al., 1993). Our limited results suggest that for explosions above a snowpack, the impact on the air pressure above the snow surface, provided changes in snow conditions are relatively small, might not be significantly different – still, the effect in terms of failure behavior might be very different.

5.10. Approximation of snowpack loading with other parameters

Snowpack accelerations are difficult to measure and these measurements require a large effort. It is therefore desirable to perform easier measurements such as the one for air pressure and use them as approximation for other parameters. The maximum vertical accelerations decreased with distance at a depth of 0.3 m $\text{kg}^{-0.65}$ with $b_{\text{acc,vert}}^{\text{X}} = 1.96$ and $b_{\text{acc,hor}}^{\text{X}} = 2.68$ (larger scatter for the horizontal component) (Table 7). The vertical accelerations were usually larger and will therefore be considered here. The maximum air pressure decreased less distinctly than the accelerations $b_{\text{airp}}^{\text{X}} = 1.68$ (Table 3). The air pressure derivative decreased in the same way with distance as the maximum air pressure (Table 4). The energy equivalent of the air pressure decreased with $b_{\text{airp,ener}}^{\text{X}} = 2.54$ (Table 5); the decrease was higher than the decrease of the maximum accelerations. The parameters maximum air pressure and air pressure energy equivalent therefore provide lower and upper bounds, respectively, for the magnitude of the decrease of the accelerations.

The maximum vertical velocities decreased in the same way as the maximum vertical accelerations with distance from the point of explosion at a given depth within the snowpack. Again, the horizontal component decreased much more pronounced. This might be due to the shallow angle of incidence which might cause waves along the surface or surface waves that have a more distinct horizontal component or waves that propagate along the snow surface. The air pressure energy equivalent provided a lower bound for the decay of the maximum horizontal accelerations. The maximum air pressure and the air pressure energy equivalent yielded lower and upper bounds for the decrease of the maximum vertical velocities. None of the coefficients describing the decrease of the air pressure and the derived parameters was close to the decrease of the energy equivalent of the snowpack velocities.

The displacements are not considered here due to extremely small values and hence no meaningful fitting parameters were obtained. There was no permanent settling observed.

5.11. Air pressure above snow and bare ground

Maximum air pressures, the air pressure derivatives and the air pressure energy equivalents above bare ground were significantly higher than above snow (Tables 3–5). Also, their decrease with distance was significantly larger above a snowpack compared to bare ground. This is expected because the hard soil reflects a higher percentage of the incoming air pressure wave than a porous, compared to soil, soft snowpack does. Albert and Orcutt (1990) reported a similar effect. Hence, it is essential to perform these types of experiments above snow despite the large operational effort required.

5.12. Lateral decrease of the air pressure

Whereas no lateral decrease was observed up to a forward cone of half angle of about 37° , the measurements along an axis perpendicular (89°) to the exploder axis showed that the air pressure and its derived parameters were significantly smaller than in axial direction (Tables 3–5). However, the decrease was less distinct compared to the gas exploder axis. The absolute values of the air pressure above snow cannot be compared to those above bare ground as described above. The relative lateral decrease, compared to the decrease in the axis of the exploder, can be compared as the snowpack is fairly uniform – as is the ground – on the entire study site.

5.13. Air pressure wave speed

Air pressure wave speeds between the three measuring pits were in good agreement with the acoustic wave velocity in air and in good agreement with the results of Simioni et al. (2015) for larger ranges outside the shock zone. Even when considering the exact location of the spark plugs within the gas exploder, speeds between the gas exploder and the first pit were unrealistically low (below 300 m s^{-1}). The reason may be that the zero time determined by the trigger of the gas exploder was not correct. It might be that there was a delay between pushing the trigger button and the ignition of the spark plug. It is therefore not clear, whether the speed of sound was exceeded at shorter distances (up to 12 m from the point of explosion). During solid explosive experiments, shock speeds were observed and the shock limit was in the range of approx. 17 to 30 m from the point of explosion.

5.14. Reproducibility

We always performed at least two experiments with approximately the same gas mass. The resulting maximal air pressure varied within 5 to 10%. Hence the results are well reproducible, even for different days with different snowpack conditions, different exploder setups and scaled gas masses.

5.15. Limitations

Our flat field experiments with an experimental gas exploder approximate a directed gas explosion comparable to an operational GAZEX® system. To ease comparison, wherever possible, the same components were used as found with an operational Gazex® gas exploder. However, there are a few distinct differences between the two systems that hinder direct comparisons. First of all, the recoil of the system might be different since operational gas exploders damp the recoil using gravity and the mass of the pipe. The system we used was tensioned with guy wires that absorb the recoil. This means that the behavior is different. However, both systems are not rigid.

Moreover, the gas masses and the derived gas volumes used with the mobile gas exploder are not necessarily the same as the volumes used to characterize the size of an operational gas exploder – though we assume that in both cases the tubes are fully filled with the turbulent mixture of the gases. In addition, our gas masses have to be considered as upper limits. It is unknown how much gas is used in operational gas exploders as they are calibrated individually via the flow time; moreover, gas amount depends on atmospheric conditions, in particular the elevation where the system is installed.

Still, we consider our gas exploder experiments as first good approximation of the effect of an operational gas exploder as we reproduced the directed explosion, used a soft system and the same gas mixture. For further validation, our results need to be compared to operational gas exploders.

6. Conclusions

We performed experiments with an experimental gas exploder above a level snow surface and bare ground. We measured air pressure at different distances from the point of explosion and snowpack accelerations at different depths within the snowpack and distances from the point of explosion.

All measurements were performed in the gas exploder axis and along a second axis to account for the non-radially symmetric shape of the pressure wave. The gas exploder was setup at different inclines and elevations above the ground. We measured the mass of the propane-oxygen gas mixture and determined a scaling factor – for maximum air pressures and gas masses. The scaling factor was 0.65 for experiments above snow and 0.4 for experiments above bare ground, which is higher than what is used with solid explosives ($\frac{1}{3}$).

The magnitude and decay of the maximum air pressure were similar along the gas exploder axis and the second axis up to angle of about 37° from the gas exploder axis. The air pressure derivatives decayed similarly as the maximum air pressure. The energy equivalent decreased more pronounced with distance than the maximum air pressure or the air pressure derivative. The maximum values as well as the decay of the air pressure with distance were in good agreement with the results reported by Simioni et al. (2015) for solid explosives.

Maximum vertical and horizontal accelerations, velocities and the energy equivalent decreased distinctly with depth within the snowpack and distance from the point of explosion as previously shown for the case of solid explosives (e.g., Binger et al., 2006; Simioni et al., 2015).

For our limited range of snowpack conditions we did not find any significant effect of snowpack properties on the air pressure above snow nor the accelerations within the snowpack; these findings do not mean that differences due to snow conditions do not exist provided they are sufficiently distinct.

Air pressures decreased significantly faster with distance above a snowpack than above bare ground. The maximum air pressures and other parameters, measured along an axis about perpendicular to the gas exploder axis, were significantly lower at short distances, but decreased less distinctly with distance than in the exploder axis. The measurements above bare ground can be used to determine the proportion of the decay laterally and to explain effects above snow. This

means, that the effect of the directed gas explosion is causing lower air pressures up to a distance of about 90 m from the explosion at 90° from the exploder axis.

The decay of the maximum air pressure or the air pressure derivative with distance gives a good lower bound for the effects within the snowpack at a certain depth; the decrease of the energy equivalent of the air pressure gives a good upper bound. Maximum displacements were very small and their fit did not lead to meaningful results due to settled snow.

Wave speeds were in the range of the speed of sound at distances larger than approx. 12 m from the point of explosion; the existence of a possible shock-wave close to the point of explosion could not be observed due to the lack of adequate instrumentation.

Due to the different characteristics of the explosions, comparing experiments with solid explosives and gas mixtures is not straightforward. However, the decay behavior with distance from the point of explosion and depth within the snowpack are similar. We conclude that in the gas exploder axis (and within an aperture angle of about 75°), the impact of a directed gas explosion is comparable to an explosion with solid explosives with similar energy density. Of course, perpendicular to the exploder axis the impact is lower. However, we found no evidence that gas explosions in general have a significantly smaller or different impact on the snowpack than explosions using solid explosives. This finding is supported by the fact that both types of explosions are extensively and successfully used in avalanche control.

Our study is the first of its kind that comprehensively examines the effect of a directed gas explosion, common to operational gas exploder systems, with a measurement setup as previously used for solid explosives. The above findings hence represent an important step towards a better understanding of the effect of a gas explosion above a snowpack – and eventually of artificially triggering avalanches.

In the future, side-by-side experiments allowing the direct comparison between gas explosions and solid explosives are needed to corroborate our findings. Moreover, measurements at operational gas exploders may help to validate our results obtained with an experimental exploder. Finally, it remains challenging to relate our measurements to the failure behavior of snow and assess consequences for avalanche release.

Acknowledgements

The study was partly funded by the Swiss Federal Office for the Environment FOEN. We would like to thank the staff of the military firing range in Hinterrhein for putting the study site at our disposal and the military forces for providing us with a crane. We thank Lino Schmid, Matthias Heck, Achille Capelli, Bettina Richter and Alec van Herwijnen for help with the field work. We thank Dan Miller for many fruitful discussions and advice on the measurement design. Two anonymous reviewers provided constructive comments, which we gratefully acknowledge. We are grateful for the support by TAS that provided the mobile gas exploder.

However, this study was performed independently of any of the manufacturers of avalanche control systems. None of the authors or other SLF staff members involved in the experiments has any affiliations with or involvement in any organization or entity with any financial interest or non-financial interest in the subject matter or materials discussed in this manuscript.

References

- Albert, D.G., 1983. Review of the propagation of inelastic pressure waves in snow. In: CRREL Report 83-13. US Army Cold Regions Research and Engineering Laboratory, Hanover NH, U.S.A.
- Albert, D.G., 2001. Acoustic waveform inversion with application to seasonal snow covers. *J. Acoust. Soc. Am.* 109 (1), 91–101.
- Albert, D.G., Hole, L.R., 2001. Blast noise propagation above a snow cover. *J. Acoust. Soc. Am.* 109 (6), 2675–2681.

- Albert, D.G., Orcutt, J.A., 1990. Acoustic pulse propagation above grassland and snow: comparison of theoretical and experimental waveforms. *J. Acoust. Soc. Am.* 87 (1), 93–100.
- Albert, D.G., Decato, S.N., Carbee, D.L., 2008. Snow cover effects on acoustic sensors. *Cold Reg. Sci. Technol.* 52 (2), 132–145.
- Berthet-Rambaud, P., 2009. Comparison of shock waves provoked by various artificial avalanche release techniques, and of their effects on the snowpack. In: Schweizer, J., van Herwijnen, A. (Eds.), *Proceedings ISSW 2009. International Snow Science Workshop, Davos, Switzerland, 27 September - 2 October 2009*. Swiss Federal Institute for Forest, Snow and Landscape Research WSL, pp. 328–329.
- Binger, J.B., Miller, D.A., 2016. Soft and hard slab snow dynamic response to explosives used in avalanche hazard mitigation. *J. Cold Reg. Eng.* 30 (2) 04015003 (17 pp.).
- Binger, C., Nelsen, J., Olson, K.A., 2006. Explosive shock wave compression in snow: effects of explosive orientation and snowpack compression. In: Gleason, J.A. (Ed.), *Proceedings ISSW 2006. International Snow Science Workshop, Telluride CO, U.S.A.* 1–6. pp. 592–597 October 2006.
- Biot, M.A., 1956. Theory of propagation of elastic waves in a fluid-saturated porous solid. I. Low-frequency range. *J. Acoust. Soc. Am.* 28 (2), 168–178.
- Bones, J., Miller, D., Savage, S., 2012. An experimental dynamic response study of hard slab seasonal snow to explosive control. In: *Proceedings ISSW 2012. International Snow Science Workshop, Anchorage AK, U.S.A.*, 16–21 September 2012, pp. 142–148.
- Bouzdidi, Y., Schmitt, D.R., 2012. Incidence-angle-dependent acoustic reflections from liquid-saturated porous solids. *Geophys. J. Int.* 191 (3), 1427–1440.
- Capelli, A., Kapil, J.C., Reiweger, I., Or, D., Schweizer, J., 2016. Speed and attenuation of acoustic waves in snow: laboratory experiments and modelling with Biot's theory. *Cold Reg. Sci. Technol.* 125, 1–11.
- Cardu, M., Chiaravallotti, L., Chiaia, B., Cornetti, P., Frigo, B., 2008. A coupled stress and energy criterion for natural and artificial triggering of dry snow slab avalanches. In: *42nd US Rock Mechanics Symposium and 2nd U.S.-Canada Rock Mechanics Symposium, San Francisco, U.S.A.*, 29 June–2 July 2008. American Rocks Mechanics Association ARMA-08-2003.
- Cooper, P.W., 1996. *Explosives Engineering*. Wiley-VCH, New York 480 pp.
- Denoth, A., 1994. An electronic device for long-term snow wetness recording. *Ann. Glaciol.* 19, 104–106.
- Fierz, C., Armstrong, R.L., Durand, Y., Etchevers, P., Greene, E., McClung, D.M., Nishimura, K., Satyawali, P.K., Sokratov, S.A., 2009. The international classification for seasonal snow on the ground, HP-VII Technical Documents in Hydrology. 83 UNESCO-IHP, Paris, France (90 pp).
- Frigo, B., Chiaia, B., Cardu, M., Giraudi, A., Godio, A., Rege, R., 2010. Experimental analysis of snowpack effects induced by blasts. In: *Proceedings ISSW 2010. International Snow Science Workshop, Lake Tahoe CA, U.S.A.*, 17–22 October 2010, pp. 66–71.
- Frigo, B., Chiaia, B., Cardu, M., 2012. Snowpack effects induced by blasts: experimental measurements vs theoretical formulas. In: *Proceedings ISSW 2012. International Snow Science Workshop, Anchorage AK, U.S.A.*, 16–21 September 2012, pp. 943–947.
- Gubler, H., 1976. Künstliche Auslösung von Lawinen durch Sprengungen. *Mitteilungen des Eidg. Inst. für Schnee- und Lawinenforschung*. Swiss Federal Institute for Snow and Avalanche Research, Davos, Switzerland 94 pp.
- Gubler, H., 1977. Artificial release of avalanches by explosives. *J. Glaciol.* 19 (81), 419–429.
- Gubler, H., Wyssen, S., Kogelnig, A., 2012. Guidelines for artificial release of avalanches. Wyssen Avalanche Control AG, Reichenbach, Switzerland, pp. 39.
- Ingram, L.F., 1962. Air blast in an arctic environment. Technical Report no. 2-597. US Army Waterways Experiment Station, Vicksburg, MS, U.S.A.
- Johnson, J.B., 1982. On the application of Biot's theory to acoustic wave propagation. *Cold Reg. Sci. Technol.* 6 (1), 49–60.
- Johnson, J.B., Solie, D.J., Brown, J.A., Gaffney, E.S., 1993. Shock response of snow. *J. Appl. Phys.* 73 (10), 4852–4861.
- Johnson, J.B., Solie, D.J., Barrett, S.A., 1994. Response of seasonal snow to explosive loading. *Ann. Glaciol.* 19, 49–54.
- Kurz, J.H., Grosse, C.U., Reinhardt, H.-W., 2005. Strategies for reliable automatic onset time picking of acoustic emissions and of ultrasound signals in concrete. *Ultrasonics* 43 (7), 538–546.
- Liebermann, E., Schippers, J., Liebermann, S.C., 2002. The "Gazex" avalanche release system. In: Stevens, J.R. (Ed.), *Proceedings ISSW 2002. International Snow Science Workshop, Penticton BC, Canada, 29 September–4 October 2002*, pp. 46–48.
- McClung, D.M., Schaerer, P., 2006. *The Avalanche Handbook*. The Mountaineers Books, Seattle WA, U.S.A. 342 pp.
- Mellor, M., 1973. Controlled release of avalanches by explosives. In: Perla, R. (Ed.), *Advances in North American avalanche technology: 1972 Symposium*. USDA Forest Service, General Technical Report RM-3, pp. 37–49.
- Miller, D.A., Tichota, R.G., Adams, E.E., 2011. An explicit numerical model for the study of snow's response to explosive air blast. *Cold Reg. Sci. Technol.* 69 (2–3), 156–164.
- Proksch, M., Rutter, N., Fierz, C., Schneebeli, M., 2016. Intercomparison of snow density measurements: bias, precision, and vertical resolution. *Cryosphere* 10 (1), 371–384.
- Sidler, R., 2015. A porosity-based Biot model for acoustic waves in snow. *J. Glaciol.* 61 (228), 789–798.
- Simioni, S., Sidler, R., Schweizer, J., Dual, J., 2014. Field measurements and modeling of wave induced weak layer failure due to an explosion. In: Haegeli, P. (Ed.), *Proceedings ISSW 2014. International Snow Science Workshop, Banff, Alberta, Canada, 29 September–3 October 2014*, pp. 722–726.
- Simioni, S., Sidler, R., Dual, J., Schweizer, J., 2015. Field measurements of snowpack response to explosive loading. *Cold Reg. Sci. Technol.* 120, 179–190.
- Stoffel, L., Nairz, P., Kleemayer, K., Procter, E., Kogelnig, A., Urschler, R., Larghi, M., Sauermoser, S., 2015. Artificial release and monitoring technologies for avalanches. In: Rudolf-Miklau, F., Sauermoser, S., Mears, A.I. (Eds.), *The Technical Avalanche Protection Handbook*. Wilhelm Ernst & Sohn, Verlag für Architektur und technische Wissenschaften GmbH & Co. KG, Berlin, Germany, pp. 325–361.
- Suriñach, E., Vilajosana, I., Kleemayer, K., Rammer, L., 2011. Study of the wavefield generated by a gas exploder used for artificial avalanche release. *Cold Reg. Sci. Technol.* 66 (1), 17–29.
- Tichota, R.G., Miller, D.A., Larson, R., Richmond, D., 2010. An experimental investigation of explosives and snowpack dynamic response. In: *Proceedings ISSW 2010. International Snow Science Workshop, Lake Tahoe CA, U.S.A.*, 17–22 October 2010, pp. 418.
- Ueland, J., 1993. Effects of explosives on the mountain snowpack. In: *Proceedings ISSW 1992. International Snow Science Workshop, Breckenridge, Colorado, U.S.A.*, 4–8 October 1992. Colorado Avalanche Information Center, Denver CO, USA, pp. 205–213.
- Withers, M., Aster, R., Young, C., Beiriger, J., Harris, M., Moore, S., Trujillo, J., 1998. A comparison of select trigger algorithms for automated global seismic phase and event detection. *B. Seismol. Soc. Am.* 88 (1), 95–106.
- Wooldridge, R.E., Hendrikx, J., Miller, D.A., Birkeland, K., 2012. The effect of explosives on the physical properties of snow. In: *Proceedings ISSW 2012. International Snow Science Workshop, Anchorage AK, U.S.A.*, 16–21 September 2012, pp. 1033–1039.